Electromagnetic Analysis of Ferrite Spoke-Type PMSM for Light-Duty EVs: A Comparison with Surface-Mounted Topology

Fatemeh Ghalavand
University of Victoria, BC
fghalavand@uvic.ca

T. Ilamparithi
University of Victoria, BC
ilampari@uvic.ca

Alireza Siadatan
York University, ON
siadatan@yorku.ca

Afshin Rezaei-Zare
York University, ON
rezaei@yorku.ca

***Abstract*—This paper presents a comparative electromagnetic analysis of spoke-type and surface-mounted permanent-magnet synchronous machines (PMSMs) for low-power, low-speed, high-torque applications. All configurations use an identical stator with double three-phase windings, while rotor topology is varied to evaluate the effects of magnet placement and flux concentration. The study assesses whether a spoke-type rotor with low-cost ferrite magnets can achieve air-gap flux density and torque performance comparable to a rare-earth surface-mounted PMSM. Finite-element analysis in Ansys is performed for three machine variants to compare electromagnetic characteristics, torque response, back-EMF, and harmonic distortion under nominal conditions. Results confirm the feasibility of ferrite-based spoke designs as a cost-effective alternative for high-torque, low-speed drives.**

***Index Terms*—PMSM, spoke-type rotor, ferrite magnet, torque.**

I. Introduction

Permanent-magnet synchronous machines (PMSMs) are widely used in electric vehicles, renewable-energy systems, robotics, and industrial automation due to their high efficiency, torque density, and dynamic response [1]. However, modern PMSM performance relies heavily on rare-earth NdFeB magnets, whose cost and availability are influenced by market volatility and supply risks [2]. This has driven growing interest in rare-earth-lean and rare-earth-free motor technologies.

Ferrite-based spoke-type PMSMs have emerged as a promising alternative by exploiting flux-concentration mechanisms to compensate for the lower remanence of ferrite magnets [3], [4]. Related approaches, including permanent-magnet-assisted synchronous reluctance machines and hybrid-excited machines, also demonstrate that competitive torque density can be achieved with reduced rare-earth content [5], [6]. Ferrite magnets additionally offer low cost and high thermal stability, making them attractive for automotive and industrial applications [7].

Despite these advances, key gaps remain. Many studies focus on surface-mounted or V-shaped ferrite rotors that do not fully utilize flux concentration, and evaluations are often limited to single operating points or incomplete performance metrics [3], [4]. Furthermore, systematic comparisons of spoke-type ferrite PMSMs with different pole numbers on a common stator platform are still scarce.

To address these gaps, this paper investigates whether a ferrite-based spoke-type PMSM can achieve competitive electromagnetic performance compared with a rare-earth surface-mounted PMSM using an identical stator and operating conditions. Finite-element simulations are used to evaluate torque, back-EMF, torque ripple, total harmonic distortion, and transient behavior, providing insight into the feasibility of spoke-type ferrite machines for high-torque, low-speed applications.

II. Geometric Design and Definition

The machine dimensions are determined using the standard electromagnetic power equation

$$P_{\text{out}} = G\, D_g^2 L_{\text{stk}}\, rps, \tag{1}$$

where G is the output coefficient, D_g is the stator inner diameter, L_{stk} is the stack length, and rps is the mechanical speed. For fixed power and speed, the dimensional product $D_g^2 L_{\text{stk}}$ remains constant, defining a trade-off between diameter and axial length.

The output coefficient is given by

$$G = \frac{1.11\pi^2 k_w B_g a_c \eta_d \cos\beta}{\gamma_{\text{emf}}}, \tag{2}$$

and the aspect ratio

$$a_r = \frac{L_{\text{stk}}}{D_g} \tag{3}$$

is used as a key design metric influencing torque capability, flux concentration, and thermal performance. A parametric sweep of D_g and L_{stk} (Fig. 1) shows that ferrite machines require a larger active volume to achieve the same air-gap flux density due to their lower remanence. Based on this analysis, $D_g = 190$ mm and $L_{\text{stk}} = 80$ mm are selected, yielding an average air-gap flux density of $B_g \approx 0.44$ T while preserving mechanical robustness. The three benchmark machines considered in this study—a surface-mounted NdFeB PMSM (S–Nd), a 20-pole ferrite spoke PMSM (Sp–F20), and a 10-pole ferrite spoke PMSM (Sp–F10)—share an identical stator geometry and operating conditions, as summarized in Table I. The spoke-type rotor topology is adopted from [8], where a dedicated flux-barrier configuration was proposed to enhance flux concentration. Their corresponding 3D geometries are shown in Fig. 2.

979-8-3315-8138-1

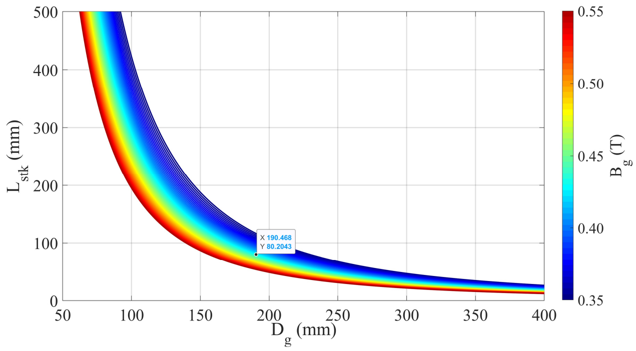

Fig. 1: Air-gap flux density B_g versus stator inner diameter D_g and stack length L_{stk}.

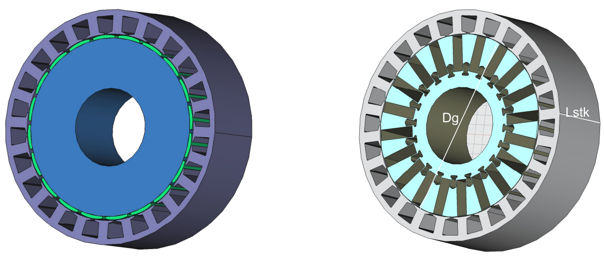

(a) Surf 20 (b) Spoke 20

Fig. 2: 3D models of the PMSM topologies studied.

A. Torque Model and Magnetization Linkage

The electromagnetic torque in the dq reference frame is expressed as

$$T_e = \frac{3}{2}p(\lambda_d i_q - \lambda_q i_d), \tag{4}$$

where p is the number of pole pairs. For surface-mounted machines ($L_d \approx L_q$), torque is dominated by the magnet flux linkage

$$T_e = \frac{3}{2}p\lambda_m i_q, \qquad \lambda_m = \lambda_d\big|_{i_d=0}. \tag{5}$$

Using the design values $p = 10$, $i_q = 4.24$ A, and $\lambda_m = 0.72$ Wb, the predicted electromagnetic torque is approximately $45.8\ \text{N}\cdot\text{m}$.

B. Material Selection

The magnetic material properties employed in the simulations are summarized in Table II. NdFeB magnets exhibit significantly higher remanence and energy product, enabling superior torque density; however, their high cost and supply-chain dependency motivate the exploration of rare-earth-free alternatives [9].

Ferrite magnets offer low cost, high thermal stability, and corrosion resistance [10]. Although their intrinsic magnetic properties are inferior to NdFeB, the use of flux-concentrating rotor topologies such as spoke-type and flux-barrier designs can substantially enhance air-gap flux density and improve demagnetization robustness, making ferrite-based machines viable candidates for traction applications [11].

TABLE I: PMSM Benchmark Configurations

Parameter	S-Nd	Sp-F20	Sp-F10
Rotor type	Surface	Spoke	Spoke
Magnet type	NdFeB	Ferrite	Ferrite
Poles	20	20	10
D_{out} (mm)	190	190	190
Stack length (mm)	80	80	80
Speed (rpm)	200	200	200
Slots	24	24	24

TABLE II: Magnetic Material Properties Used in Analysis

Property	NdFeB (N35)	Ferrite (Y30)
Remanence B_r (T)	1.23	0.40
Coercivity H_c (kA/m)	890	250
Recoil permeability μ_r	1.05	1.10
Max. energy product $(BH)_{\text{max}}$ (kJ/m^3)	280	32
Density (g/cm^3)	7.5	5.0
Approx. cost (USD/kg)	80–100	2–5

III. FEA Modeling Assumptions

A. Materials and Magnetic Models

Electrical steels: Nonlinear B–H curves from manufacturer data are used to model the stator and rotor cores. Iron losses are included via frequency-dependent Steinmetz coefficients, accounting for both hysteresis and eddy-current effects.

Magnets: NdFeB and ferrite magnets are modeled using their recoil (demagnetization) characteristics, expressed as

$$\mathbf{B} = \mu_0(\mathbf{H} + \mathbf{M}), \qquad \mathbf{M} = \mathbf{M}_r + \chi\mathbf{H},$$

where $\mathbf{M}$ (A/m) is the magnetization and χ the differential susceptibility. Temperature coefficients for $B_r(T)$ and $H_c(T)$ capture thermal degradation, and demagnetization safety is verified by ensuring

$$\mathbf{H} \cdot \hat{m} > -H_{\text{c,irr}}.$$

B. Winding, Current Loading, and Operating Points

The per-phase flux linkage is

$$\psi_m = k_w N \phi_1, \qquad \phi_1 \approx \bar{B}_g A_{\text{pole}},$$

with k_w the winding factor and $\bar{B}_g$ the average air-gap flux density. Surface machines exhibit negligible saliency, whereas spoke-type ferrite rotors show pronounced *d*/*q* inductance asymmetry due to their flux-barrier geometry. All machines are evaluated under identical current density and thermal limits. Flux-weakening is achieved by applying negative i_d to maintain DC-bus voltage compliance at higher speeds.

C. Pole Number and Magnet Geometry Coupling

The mechanical pole pitch $\tau_p = \pi D_r/p$ (with rotor diameter D_r and pole pairs p) sets the available magnet arc length. For equivalent fundamental $\bar{B}_g$, ferrite spoke designs exploit (i) larger magnet area and (ii) flux-concentration ratio γ:

$$\Phi_{\text{Nd}} \simeq \lambda B_r^{\text{Nd}} A_m^{\text{Nd}} \;\approx\; \lambda_c B_r^{\text{Fe}} A_m^{\text{Fe}} \gamma = \Phi_{\text{Fe}}, \tag{6}$$

979-8-3315-8138-1

with leakage factors λ, λ_c, magnet area per pole A_m, and $\gamma > 1$ from spoke flux guidance. The 10-pole machine (larger τ_p) admits longer magnets than the 20-pole case, easing ferrite substitution.

D. Meshing and Solver Settings

A 2-D transient magnetic FEA is performed with adaptive mesh refinement in: (i) air gap, (ii) stator tooth tips, (iii) rotor bridges, and (iv) magnet edges. Target element size in the air gap is set to resolve at least 20–30 elements per electrical wavelength of the fundamental. Time stepping resolves at least $N_t \geq 360/\Delta\theta_e$ steps per electrical cycle (typ. $\Delta\theta_e \leq 2°$). End effects are accounted for via effective stack-length factor or 2.5D correction.

E. Boundary Conditions and Symmetry

Periodic (anti-)symmetry boundary conditions are applied over $360°/P$ sectors. The outer stator boundary is set to magnetic insulation (Dirichlet $A_z = 0$) or infinite-element shell. Slot currents are imposed as sinusoidal dq equivalents or coil-lumped excitations with phase shift 120° (or multi-phase if applicable).

IV. FEA Results

A. No-Load Back-EMF and Harmonic Content

The no-load back-EMF waveform serves as a key indicator of a PMSM's electromagnetic quality and flux linkage accuracy. The phase back-EMF $e_a(t)$ and its fundamental amplitude E_1 are used to validate the analytical prediction of flux linkages in the air gap. The RMS back-EMF per phase is given by

$$E_{\text{ph,rms}} = \frac{E_1}{\sqrt{2}} = \frac{\omega_e \psi_m}{\sqrt{2}}, \tag{7}$$

where ω_e and ω_m denote the electrical and mechanical angular speeds, respectively, and ψ_m is the flux linkage per phase. Fig. 3 compares the no-load line-to-line back-EMF of the three machines. The surface-mounted NdFeB PMSM produces the most sinusoidal waveform with the highest amplitude, while the 20-pole ferrite spoke design shows slightly increased magnitude with mild distortion due to flux concentration. The 10-pole spoke machine exhibits lower EMF amplitude, consistent with its reduced electrical frequency, yet maintains acceptable waveform quality.

Harmonic Analysis: The harmonic content of the back-EMF is evaluated using the total harmonic distortion (THD),

$$\text{THD} = \frac{\sqrt{\sum_{n=3,5,\ldots} E_n^2}}{E_1} \times 100\%, \tag{8}$$

where E_n denotes the nth harmonic component. Fig. 4 presents the harmonic amplitude spectra of the three machines.

The Surf20 machine exhibits a dominant fundamental component and minimal harmonic content, while the S20 configuration shows slightly elevated low-order harmonics (primarily 3rd and 5th), characteristic of flux-concentrating rotors. The S10 machine presents the lowest overall harmonic magnitudes, attributed to its pole-slot combination and reduced electrical frequency. Correspondingly, the THD values are **2.90%** (Surf20), **3.26%** (S20), and **1.55%** (S10).

The phase spectra in Fig. 5 indicate that Surf20 maintains more uniform harmonic phase alignment, whereas the spoke-type machines exhibit greater dispersion. Nevertheless, the overall waveform quality of all designs remains suitable for vector-controlled operation.

B. Torque Analysis

Reluctance Torque Fig. 6 shows the reluctance torque contributions. As expected, the surface-mounted NdFeB machine exhibits a negligible reluctance torque component, confirming its non-salient structure. The spoke-type ferrite machines generate a clear reluctance torque due to rotor saliency and flux-barrier geometry. The 20–pole spoke design achieves a higher reluctance torque level ($\approx$ 2.9 Nm) compared to the 10–pole variant ($\approx$ 1.2 Nm).

dq Torque Fig. 7 illustrates the dq torque waveform. The surface NdFeB machine generates approximately 44.5 Nm average dq torque, while the 20–pole ferrite spoke topology achieves a comparable value of 49.5 Nm due to flux–focusing effects. The 10–pole ferrite design produces a lower torque level ($\approx$ 31.3 Nm) consistent with reduced flux utilization. Minimal ripple is observed in the surface machine, whereas the spoke ferrite machines exhibit higher torque ripple due to saliency–induced harmonics.

The total torque comparison in Fig. 8 confirms the expected performance ranking:

$$T_{\text{20p-Nd}} \approx 44.5 \text{ Nm} < T_{\text{20p-F}} \approx 49.5 \text{ Nm} > T_{\text{10p-F}} \approx 31.3 \text{ Nm}.$$

The 20–pole ferrite spoke machine achieves the highest average torque among the three designs, demonstrating the effectiveness of flux–focusing. The surface machine maintains extremely low ripple ($< 0.15\%$), while the spoke ferrite designs show higher ripple levels ($\approx 5.9\%$ and 7.4%), consistent with increased saliency.

C. Dynamic Performance Evaluation

Fig. 9 shows the torque–speed characteristics of the three PMSM topologies under rated current with field weakening enabled. All machines exhibit the classical two-region PMSM behavior: a constant-torque region followed by a field-weakening region where torque decreases due to voltage limitations.

The S20 machine (Fe, 20P) delivers the highest constant torque (about 49.5 N·m) up to roughly 225 rpm, after which torque declines rapidly due to its higher back-EMF and increased q-axis inductance, which reduce the voltage margin. By approximately 245 rpm, the torque falls below 30 N·m, indicating an early onset of field weakening.

The Surf20 machine (Nd, 20P) produces around 44.5 N·m up to about 240 rpm, after which torque also decreases sharply. This behavior reflects its lower back-EMF compared to S20, although the field-weakening range remains relatively narrow.

979-8-3315-8138-1

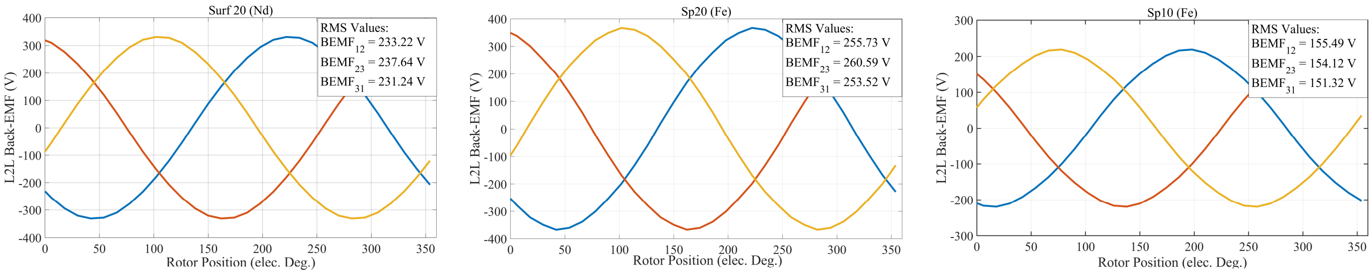

(a) Surface PMSM (20 poles) (b) Spoke PMSM (20 poles) (c) Spoke PMSM (10 poles)

Fig. 3: Line-to-line back-EMF waveforms at rated speed for the three PMSM designs.

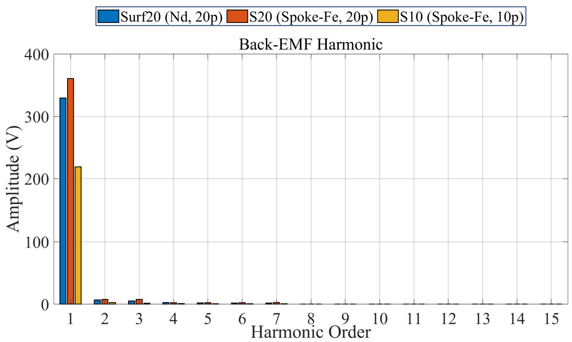

Fig. 4: Back-EMF harmonic amplitude comparison for the Surf20, S20, and S10 machines.

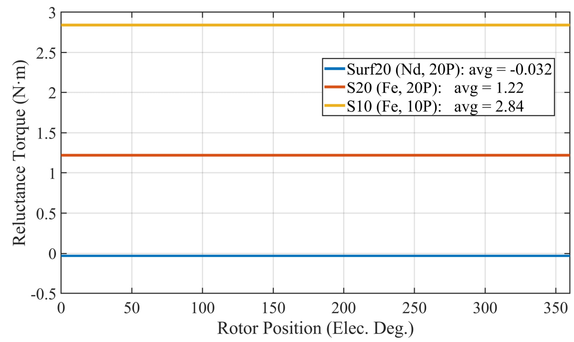

Fig. 6: Reluctance torque comparison of the three machines.

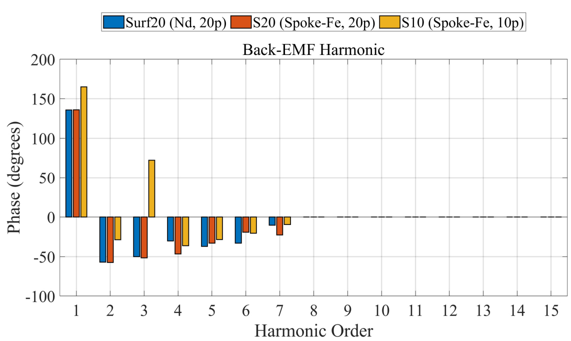

Fig. 5: Back-EMF harmonic phase comparison for the Surf20, S20, and S10 machines.

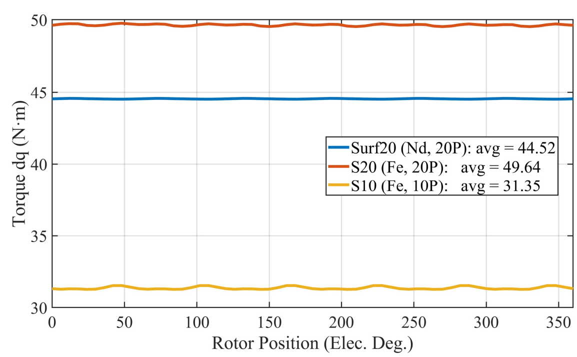

Fig. 7: dq torque comparison of the three machines.

The S10 machine (Fe, 10P) generates a lower constant torque of approximately 31.5 N·m but sustains this level up to around 295 rpm. Torque then decreases more gradually, reaching zero near 340 rpm, due to its reduced magnet flux and delayed voltage saturation.

Overall, the S20 topology offers the highest torque density with a limited speed range, Surf20 provides a balanced compromise, and S10 achieves the widest speed range, making it suitable for extended constant-power operation.

Fig. 10 presents the corresponding power–speed characteristics, where all machines reach similar peak power near base speed, confirming consistent sizing.

The ferrite-based spoke machines (S20 and S10) achieve power levels comparable to the NdFeB-based Surf20, demonstrating the feasibility of rare-earth-free designs. While S10 exhibits lower power at low speed due to reduced torque, this

979-8-3315-8138-1

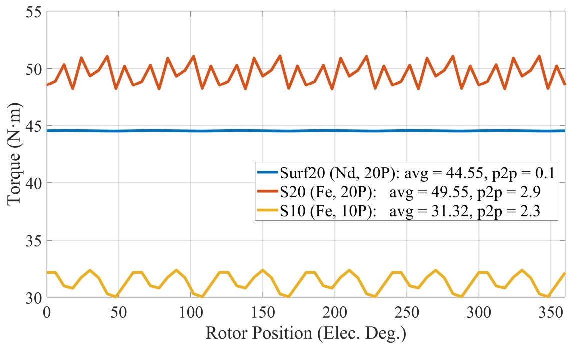

Fig. 8: Total torque comparison of the three machines.

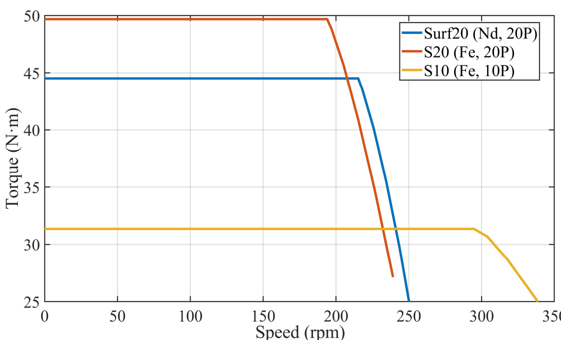

Fig. 9: Torque–speed characteristics of the three PMSM topologies under rated current operation.

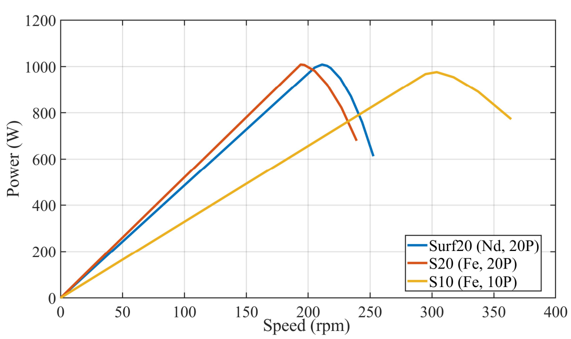

Fig. 10: Power–speed characteristics of the three machines under rated current with field weakening.

is offset by superior high-speed capability enabled by its lower flux linkage.

V. Conclusion

This study presented a comparative analysis of ferrite-based spoke-type PMSMs and a surface-mounted NdFeB PMSM using an identical stator platform. The 20-pole ferrite spoke machine demonstrated higher torque than the surface-mounted machine, confirming that flux-concentrating rotor architectures can effectively compensate for the lower remanence of ferrite magnets. The spoke-type designs exhibited slightly higher torque ripple and harmonic content, but the waveforms remained suitable for vector-controlled operation. Overall, the results indicate that ferrite-based spoke-type PMSMs can achieve competitive electromagnetic performance while substantially reducing magnet cost, making them a promising rare-earth-free alternative for low-speed, high-torque applications. Future work may explore further optimization of rotor geometry and pole count to enhance torque density and efficiency.

Acknowledgment

The authors gratefully acknowledge the University of Victoria and NSERC for financial support, and CMC Microsystems, through the FABrIC project funded by the Government of Canada, for providing CAD pass access to CAD tools that supported motor design and electromagnetic simulation.

References

[1] B. Podmiljšak, P. Virtic, and B. Stumberger, "The future of permanent-magnet-based electric motors," *Progress in Electromagnetics Research M*, vol. 120, pp. 157–166, 2024.

[2] O. M. Lee, J. H. Lee, S. Kim, and D. Hyun, "Reducing rare-earth magnet reliance in modern traction electric machines," *Energies*, vol. 18, no. 9, p. 2274, 2025.

[3] P. C. K. Luk, "Low-cost high-performance ferrite permanent magnet machines: A viable replacement for rare-earth machines?," *eTransportation*, vol. 5, p. 100070, 2020.

[4] G. Artetxe, I. Otxotorena, M. A. Gracia, M. Igarzabal, and X. Kortabarria, "Eliminating rare earth permanent magnets on low-speed high-torque applications," *IET Electric Power Applications*, vol. 15, no. 6, pp. 727–737, 2021.

[5] R. Qu and T. A. Lipo, "Design optimization of PM-assisted synchronous reluctance machines," *IEEE Trans. Ind. Appl.*, vol. 50, no. 4, pp. 2331–2342, 2014.

[6] K. H. Shin, S. Kim, I. Jeong, S. H. Jang, and H. Kim, "Hybrid-excited synchronous machine to reduce rare-earth magnets for electric vehicles," *IEEE Trans. Energy Convers.*, vol. 37, no. 4, pp. 2875–2885, 2022.

[7] Y. Miyama, R. Ogawa, and K. Sakamoto, "Development of rare-earth-free ferrite permanent magnet motors for automotive applications," in *SAE Technical Paper*, no. 2021-01-0753, 2021.

[8] F. Ghalavand and T. Ilamparithi, "High-performance spoke-type PMSM rotor for high-torque, low-speed applications," in *Proc. IEEE/AIAA ITEC-EATS*, Indianapolis, IN, USA, 2025.

[9] Z. Chen and D. Xu, "Permanent Magnet Materials and Their Applications," *Springer*, 2018.

[10] J. M. D. Coey, "Permanent magnet applications," *Journal of Magnetism and Magnetic Materials*, vol. 248, pp. 441–456, 2002.

[11] P. Sergeant and R. V. Sabariego, "Torque and power capability of ferrite PM machines using flux concentration," *IEEE Trans. Ind. Electron.*, vol. 68, no. 11, pp. 10865–10875, 2021.

979-8-3315-8138-1